Latin American Journal of Aquatic Research

E-ISSN: 0718-560X

lajar@pucv.cl

Pontificia Universidad Católica de Valparaíso

Chile

Andrade, Isabel; Hormazábal, Samuel; Combes, Vincent

Intrathermocline eddies at the Juan Fernández Archipelago, southeastern Pacific Ocean

Latin American Journal of Aquatic Research, vol. 42, núm. 4, octubre, 2014, pp. 888-906

Pontificia Universidad Católica de Valparaíso

Valparaíso, Chile

Lat. Am. J. Aquat. Res., 42(4): 888-906, 2014
"Oceanography and Marine Resources of Oceanic Islands of Southeastern Pacific"
M. Fernández & S. Hormazábal (Guest Editors)
DOI: 10.3856/vol42-issue4-fulltext-14

Research Article

Intrathermocline eddies at the Juan Fernández Archipelago, southeastern Pacific Ocean

Isabel Andrade[1], Samuel Hormazábal[1] & Vincent Combes[2]
[1]Escuela de Ciencias del Mar, Pontificia Universidad Católica de Valparaíso
P.O. Box 1020, Valparaíso, Chile
[2]College of Oceanic and Atmospheric Sciences, Oregon State University, Corvallis, Oregon, USA

ABSTRACT. Regional Ocean Modeling System (ROMS) results, combined with chlorophyll-*a* (Chl-*a*) and satellite altimetry information as well as information from oceanographic cruises were analyzed to identify interactions between intrathermocline eddies (ITEs) and the Juan Fernández Archipelago (JFA), and discuss their potential impact on surface Chl-*a* concentrations. The JFA is located off the coast of central Chile (33°S), and is composed of three main islands: Robinson Crusoe (RC), Alejandro Selkirk (AS) and Santa Clara (SC). Results indicate that the surface and subsurface anticyclonic eddies that interact with the JFA are formed primarily within the coastal transition zone between 33° and 39°S. ITEs are present within the JFA region with a semiannual frequency, mainly during the austral autumn, and have a weak surface expression in relation to the adjacent surface eddies, with a slow displacement (1.16 to 1.4 km d^{-1}) in a northwest direction and a coherent structure for periods of ≥1 year. During the ITEs' interaction with RC-SC islands and an adjacent seamount, a slight (prominent) thermocline deflection of the upper limit (lower) was observed. The horizontal extent (~70-100 km) was greater than the internal Rossby deformation radius and the average vertical extent was ~400 m. The interaction between the weak surface expression of ITEs, identified with satellite altimetry, and the JFA persisted during autumn for nine weeks until reaching the winter period. Approximately one month after the beginning of the interaction between ITEs and the islands, increases in surface Chl-*a* associated with the eddy were observed, with values up to three times higher than adjacent oceanic waters.

Keywords: intrathermocline eddies, Juan Fernández Archipelago, southeastern Pacific Ocean.

Remolinos intratermoclina en el Archipiélago Juan Fernández, Océano Pacífico suroriental

RESUMEN. Se analizaron los resultados de un modelo oceánico regional (ROMS), combinado con información de clorofila-*a* (Clo-*a*) y altimetría satelital, además de información proveniente de cruceros oceanográficos, para identificar la interacción entre los remolinos intratermoclina (ITEs) y el Archipiélago Juan Fernández (AJF), y discutir su potencial impacto sobre las concentraciones de Clo-*a* superficial. El AJF se encuentra ubicado frente a la costa central de Chile (33°S), y está conformado por las islas Robinson Crusoe, Santa Clara y Alejandro Selkirk. Los resultados indican que los remolinos anticiclónicos superficiales y subsuperficiales que interactúan con el AJF se forman principalmente en la zona de transición costera entre 33° y 39°S. Los ITEs se presentan en la región del AJF con una frecuencia semianual, principalmente durante el período de otoño austral, y poseen una débil expresión superficial respecto de los remolinos superficiales adyacentes, un lento desplazamiento (1,16-1,4 km d^{-1}) con dirección noroeste y una estructura coherente por períodos ≥1 año. Durante la interacción de los ITEs con las islas RC-SC y el monte submarino adyacente, se observó una leve (prominente) deflexión del límite superior (inferior) de la termoclina. La escala horizontal (~70-100 km) fue mayor que el radio interno de deformación de Rossby y la escala vertical promedio fue de ~400 m. La interacción entre el ITE de débil expresión superficial identificada con altimetría satelital durante el período de otoño y el AJF perduró durante nueve semanas alcanzando el período invierno. Aproximadamente un mes después del comienzo de la interacción entre el ITE y las islas, se observaron incrementos de Clo-*a* superficial asociados al remolino con valores hasta tres veces mayores, respecto de las aguas oceánicas adyacentes.

Palabras clave: remolinos intratermoclina, Archipiélago Juan Fernández, Océano Pacífico suroriental.

Corresponding author: Isabel Andrade (isabelandradec@gmail.com)

INTRODUCTION

Intrathermocline eddies (ITEs) are mesoscale vortices characterized by a lens-like shape with maximum velocity 200-300 m below the thermocline (Dugan *et al.,* 1982; Gordon *et al.,* 2002; Colas *et al.,* 2011). Each ITE plays an important role in the transport of coastal waters into the deep ocean (~1 Sv) and can live for several years (Filyushkin *et al.,* 2011a; Nauw *et al.,* 2006). ITEs have already been observed and named according to their region of origin: "Cuddies" off California (Garfield *et al.,* 1999), "Meddies" on the slope of the Iberian Peninsula (Armi & Zenk, 1984), "Swoddies" in the Bay of Biscay (Pingree & Le Cann, 1992), "Reddies" in the Red Sea (Shapiro & Meschanov, 1991) or "UWE" for the ITEs formed in the Ulleung Basin in the southeastern area of the East Sea of Japan (An *et al.,* 1994). In the southeast Pacific, the spatial structure and origin of these eddies have been previously identified and characterized using Argo float data (Johnson & McTaggart, 2010), oceanographic cruises (Morales *et al.,* 2012), satellite altimetry and numerical model results (Chaigneau *et al.,* 2011; Colas *et al.,* 2011; Hormazábal *et al.,* 2013). It has been postulated that, off the coast of Chile, the ITEs would be formed in the Coastal Transition Zone (CTZ; Hormazábal *et al.,* 2004) mainly during the austral spring-summer (Hormazábal *et al.,* 2013), when the wind stress is favorable for coastal upwelling. ITEs are generally triggered by the instability of the Perú-Chile Undercurrent (PCUC) but can also been altered by a change of coastal upwelling which induces a change of zonal density gradient (*i.e.,* vorticity) (Leth & Shaffer, 2001; Hormazábal *et al.,* 2004, 2013; Colas *et al.,* 2011). When the ITEs detach from the PCUC, they transport high-nutrient and low-oxygen concentrations from the Equatorial Subsurface Water (ESSW) into the open ocean (Johnson & McTaggart, 2010; Hormazábal *et al.,* 2013). Previous studies estimated a transport on the order of ~1Sv per ITE (Hormazábal *et al.,* 2013). Similar to surface-intensified eddies, ITEs can also modify productivity offshore through the transport of nutrient-rich ESSW waters. Previous studies have also reported that the mixing of waters within the ITEs core redistributes the water column's chemical properties and impacts the phytoplankton surface concentration (McGillicuddy *et al.,* 1998, 2007; Bakun, 2006; Siegel *et al.,* 2011). In the southeastern Pacific, the impact of the ITEs on the biological-pelagic system in the open ocean remains unclear. In particular, the interaction of the ITEs with bathymetric features (*e.g.,* islands, seamounts) has not been assessed. We argue that ITEs generated off central Chile affect the water properties within the Juan Fernández Archipelago, favoring the horizontal and vertical transport of nutrients/heat known as eddy pumping, that corresponds to one of the mechanisms associated with the biological production increase at these oceanic zones (Falkowski *et al.,* 1991; Aristegui *et al.,* 1997; McGillicuddy *et al.,* 2007).

In Chile, the Juan Fernández Archipelago is located ~650 km off the coast of Valparaíso (~33°S) and consists of three islands of volcanic origin (González-Ferrán, 1987): Robinson Crusoe (RC), Santa Clara (SC) and Alejandro Selkirk (AS). This archipelago is the surface expression of an underwater ridge with an east-west orientation ~424 km in length, beginning at Bajo O'Higgins seamount (~72°W) and ending in a seamount located immediately west of the AS island (~83°W). Around RC, SC and AS islands, a high biological production (*e.g.,* fish, crustaceans; Rozbaczylo & Castilla, 1987; Pequeño & Sáez, 2000; Landaeta & Castro, 2004) has been observed, associated with high chlorophyll-*a* (Chl-*a*) concentrations (Pizarro *et al.,* 2006; Andrade *et al.,* 2012, 2014). Also known as Island Mass Effect (Doty & Ogury, 1956), the increase of local Chl-*a* in the vicinity of these islands results from the increase of nutrients in the euphotic zone from the interaction between mesoscale eddies and island topography (Andrade *et al.,* 2012, 2014). The goal of this study is to identify and characterize the interaction between ITEs generated in CTZ off Chile with the Juan Fernández Archipelago and to discuss the potential impact on surface Chl-*a* concentrations observed at the archipelago.

MATERIALES AND METHODS

Satellite data

Satellite Chl-*a* and geostrophic currents derived from satellite altimetry are used to evaluate the spatial and temporal trajectory of anticyclonic eddies generated in the CTZ, their interaction with the Juan Fernández Archipelago, and the potential effect on Chl-*a* concentrations. We used daily Chl-*a* data from the level-2 MODIS Aqua product (http://www.oceancolor web.com). The Chl-*a* data has a spatial resolution of 1 km and was analyzed for the period 2002-2007. Gaps in the Chl-*a* time series due to clouds were filled using a "Data Interpolating Empirical Orthogonal Function" (DINEOF) method (Beckers & Rixen, 2003; Alvera-Azcárate *et al.,* 2005, 2007). The weekly geostrophic currents (0.25° resolution) were derived from the AVISO sea surface height anomaly (http://www.aviso.oceanobs.com/).

The eddy tracking method and eddy radius were based on the closed contours of Okubo-Weiss parameter (W; Isern-Fontanet *et al.,* 2004), which is derived from geostrophic currents. We defined as "eddy" any closed W contour of $-5x10^{-12}$ s^{-2} with a

diameter greater than 50 km (Correa-Ramírez *et al.,* 2007; Morales *et al.,* 2012; Hormazábal *et al.,* 2013). The cyclonic and anticyclonic rotation directions were determined by the sign of the vorticity.

Hydrographic data

Observed ITEs off central Chile were characterized by vertical sections of temperature (°C), salinity, density (sigma-t) and dissolved oxygen (mL L^{-1}) obtained through CTD measurements between 0 and 600 m. Measurements were made during a research cruise conducted between June 2nd and June 28th, 2006 by the Banco Integrado de Proyectos (BIP). The area considered for the cruise was between 32°-44°S to 72°-86°W, within which a total of 21 transects were performed (not shown). Transects conducted during the cruise reported 13 ITEs within the CTZ and only 1 reaching the Juan Fernández Archipelago. This ITE was observed in transect N°6 at 37°05'S and between 75°-77°W (Figs. 1-2).

Data model

To further describe the ITEs off Central Chile, we examined the solution of a model experiment. The model used in this study was the Regional Ocean Modeling System (ROMS). ROMS is a three dimensional, free surface, hydrostatic, eddy-resolving primitive equation ocean model with orthogonal curvilinear coordinates in the horizontal and terrain-following coordinates in the vertical (Shchepetkin & McWilliams, 2005). We used the AGRIF version of ROMS (http://roms.mpl.ird.fr/), which offers the capability of a 2-way nesting procedure with a high resolution "child" model embedded into a coarser resolution "parent" model (Fig. A1; Debreu *et al.,* 2011).

The parent grid encompassed the central Chile region (40°-24.8°S, 85°-70°W), had a spatial resolution of 1/20° (~4.6 km) and 40 vertical levels, with enhanced resolution at the surface. The child grid extended eastward from 82° to 76°W and northward from 35.7° to 31.5°S (Fig. A1). The child grid had a spatial resolution of 1/60° (~1.5 km) and 40 vertical levels. This configuration allowed the generation of ITEs at the coast within the parent grid and propagation into the higher resolution child grid afterward. Within the child grid, the ITEs could interact with the bottom bathymetry at 1/60° resolution. The bottom topography was a smooth version of the ETOPO1 dataset (Amante & Eakins, 2009).

At the surface the model was forced by daily QuickSCAT wind stress and climatological heat and fresh water fluxes from the COADS dataset (Da Silva *et al.,* 1994). At the lateral open boundaries of the parent grid, we imposed a modified radiation boundary condition (Marchesiello *et al.,* 2001) with adjustment to the monthly mean climatology provided by the high-resolution MOM3-based Ocean General Circulation Model code optimized for the Earth Simulator (OFES; global 0.1° ocean circulation model, Masumoto *et al.,* 2004; Sasaki *et al.,* 2004, 2008). The initial condition was obtained from the OFES global ocean model for the month of January. The model was run from January 2000 to December 2007. Throughout this section, we will analyze the result of the child grid only. Some validation of the model experiment is shown Appendix A.

To identify the model ITEs' main spatial and temporal variability in the study region, we applied a the MultiTaper Method-Singular Value Descomposition (MTM-SVD) method, which combines the multitaper method (Multitaper Method, MTM), and the singular value decomposition method (Singular Value Descomposition, SVD), which allows the description of spatial characteristics for the frequencies of interest through reconstruction (Mann & Park, 1999; Correa-Ramírez & Hormazábal, 2012). A detailed guide to the features of the aforementioned method can be found in Correa-Ramírez & Hormazábal (2012).

RESULTS

ITEs observation off the coast of Chile

Figure 2 shows the vertical profile of temperature, salinity, density and dissolved oxygen along transect N°6 (37°05'S) during June 2006. Around 100-170 nm from the coast, the data indicate the presence of an ITE. Consistent with previous hydrographic studies (Hormazábal *et al.,* 2013), this ITE is associated with a bi-convex lens shape density, high salinity core (>34.5), low oxygen (<1 mL L^{-1}) and a depression of the isotherm below the thermocline. Although most of the ITEs show similar characteristics, their vertical structure may strongly depend on the PCUC vorticity and local wind stress curl (Colas *et al.,* 2011; Hormazábal *et al.,* 2013). To describe the trajectory of this particular eddy, we used the AVISO satellite sea surface height. Figure 3 shows the evolution of the geostrophic current derived from June 2006 to May 2007. Although the surface expression is weak during its initial phase, the tracking method can be used to follow the eddy for ~1 year. Compared to previous observed ITE, this ITE has a slow (~1.16 km d^{-1}) northwest displacement and reaches the southwest part of the AS after 49 weeks and ~400 km. Note that the surface expression of ITEs weakens while the ITEs move westward below the thermocline (which deepens

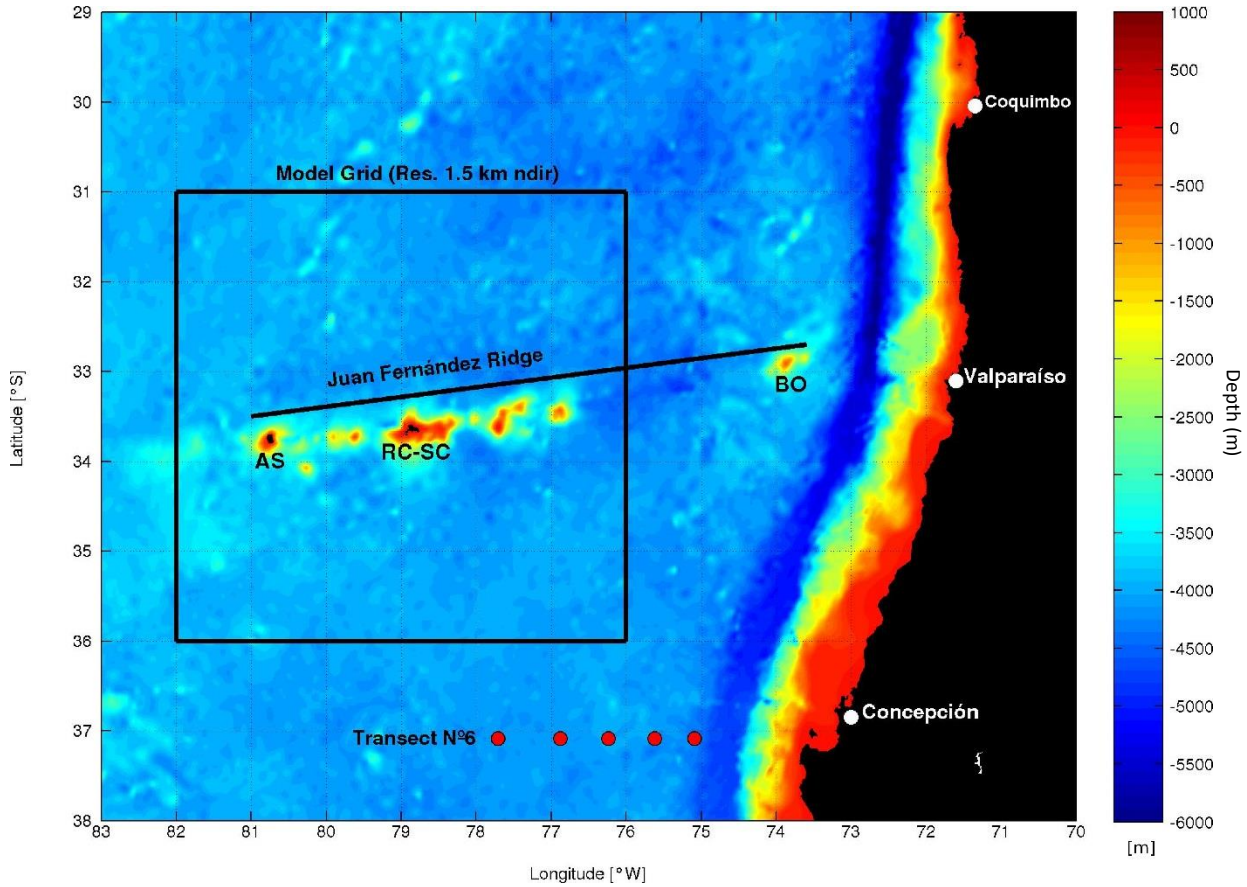

Figure 1. Bathymetry of the study area considered by the Regional Oceanic Modelling System "ROMS" (black box), nested within the global model OFES. The modeled region extends from 31°-36°S and 76°-82°W. The figure shows the full extent of the Juan Fernández Ridge, highlighting the western fraction of the Alejandro Selkirk Island (AS), the Robinson Crusoe-Santa Clara islands (RC-SC), and Monte Bajo O'Higgins (BO) at the eastern fraction. The red dots represent the position of transect N°6 during the BIP-2006 research cruise performed between June 2-28 by the Bank of Fisheries Research (BIP).

westward). Nonetheless the ITEs are still strong below the surface, as recorded with Argo floats data.

Model ITEs in the Juan Fernández Archipelago (JFA)

To better describe the ITEs reaching the JFA, we analyzed the high-resolution model solution. Several ITEs have been generated by the instability of the PCUC from 2000 to 2007. Of these eddies, one reached the JFA on March 2003 (Fig. 4). It is worth mentioning that the model does not assimilate field data. Therefore, we do not expect good agreement between the positions of the model and observed eddies. Figure 4 shows the presence of two ITEs interacting with the JFA during austral autumn (labeled "R1" (~78.5°W) and "R2" (~76.6°W)). The characteristics of R1 and R2 are detailed in Table 1. Both eddies have properties consistent with the observations described previously, with maximum salinity ~250 m (>34.4), warmer core and depression of the ispycnals below the thermocline. Both eddies have a similar transport of ~0.5 Sv, which is lower that the ~1 Sv estimate from Hormazábal *et al.* (2013). Finally, the core of these ITEs is deeper than the ITEs observed in the CTZ off central Chile (Morales *et al.,* 2012; Hormazábal *et al.,* 2013), as they propagate below the thermocline.

Table 1. Features of the R1 and R2 ITEs identified with outputs of the regional ocean model nested within the study region for the date 2002-03-22.

Features of eddies	R1	R2
Horizontal area [km^2]	3526	7854
Upper limit [m]	207	220
Lower limit [m]	683	551
Height [m]	476	331
Width [km]	67	100
Average transport [Sv]	0.5	0.51

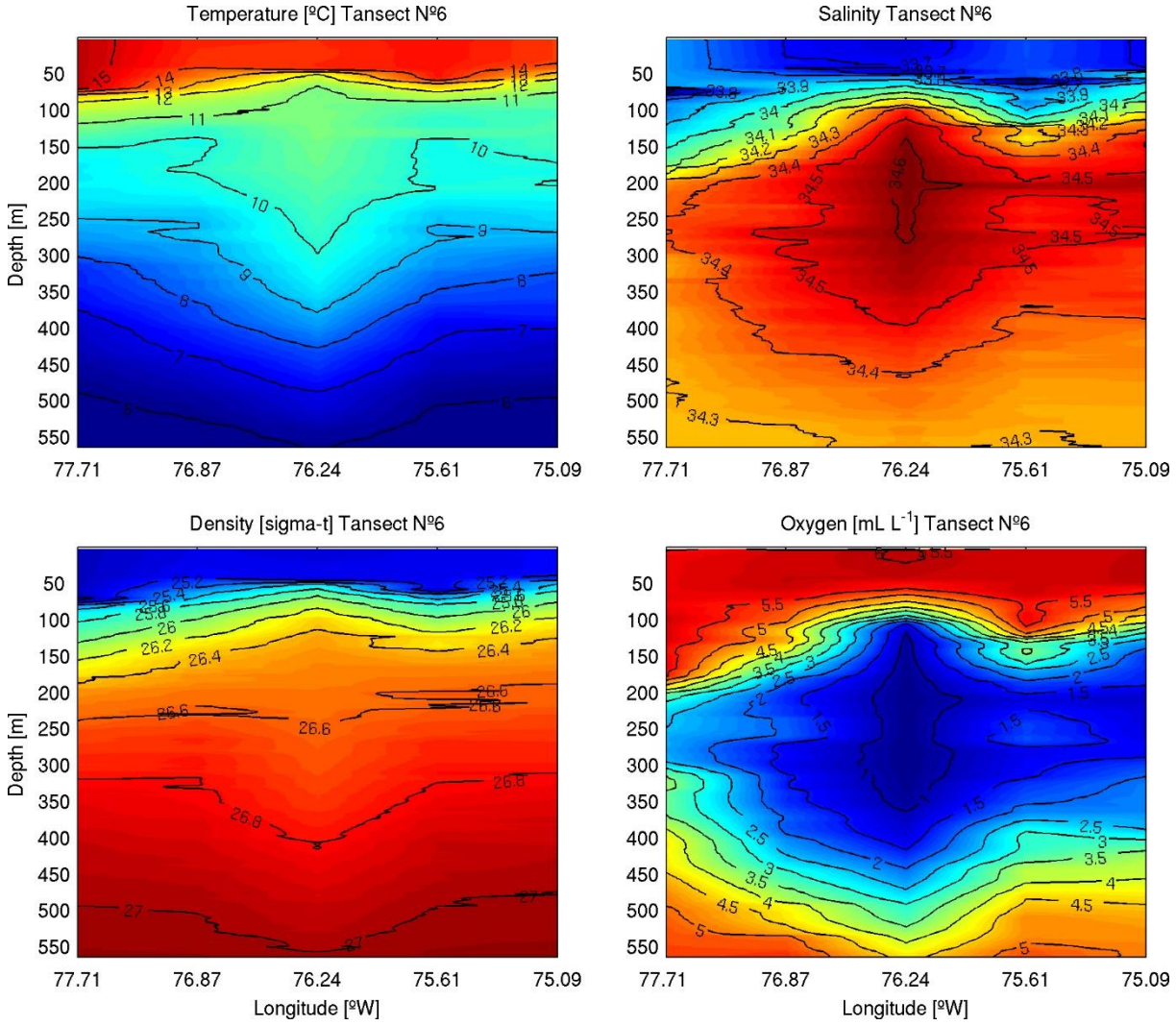

Figure 2. Vertical sections (0-600 m) of temperature (°C), salinity, density (sigma-t) and dissolved oxygen (mL L^{-1}) at 37°05'S obtained through measurements with CTD during the BIP-2006 research cruise performed between June 2-28. Dotted lines represent the location of the five stations from transect N°6 taken by the cruise (Fig.1).

However, the differences between R1 and R2 are important in the horizontal. Figure 5 shows the salinity distribution at 50 m (~euphotic layer depth) and 250 m (depth of the ITEs). While R2 is a well-defined rounded eddy, R1 presents a more elongated deformation. This shows the trajectory of the ESSW waters transported by ITEs after interacting with the RC-SC islands and adjacent seamounts. Note that R1 has a higher surface salinity than that presented by R2, a difference associated with the vertical elevation of the isohalines produced by the interaction of R1 with the dorsal's topography (Figs. 4-5). The R1 surface expression at 50 m deep suggests that the interaction between the eddy and topography may favor the ascent of the nutricline within the euphotic layer and may also inject the nutrients needed to promote an increase in phytoplankton population.

Eddies and chlorophyll-*a* satellite data around the Juan Fernández Archipelago

With a mean velocity of ~2 km d^{-1} (Hormazábal *et al.,* 2013), it takes around six months to the ITE travel from the CTZ to the JFA. Since ITEs tend to begin during the spring season (CTZ), it is more likely to observe ITEs in the vicinity of the JFA in the autumn.

We have therefore listed all the anticyclonic eddies with weak surface expression crossing the JFA during autumn. Figure 6 shows the trajectory of one particular eddy, which agrees the previous criteria. While it is not certain this anticyclone is an ITE, it was first detected

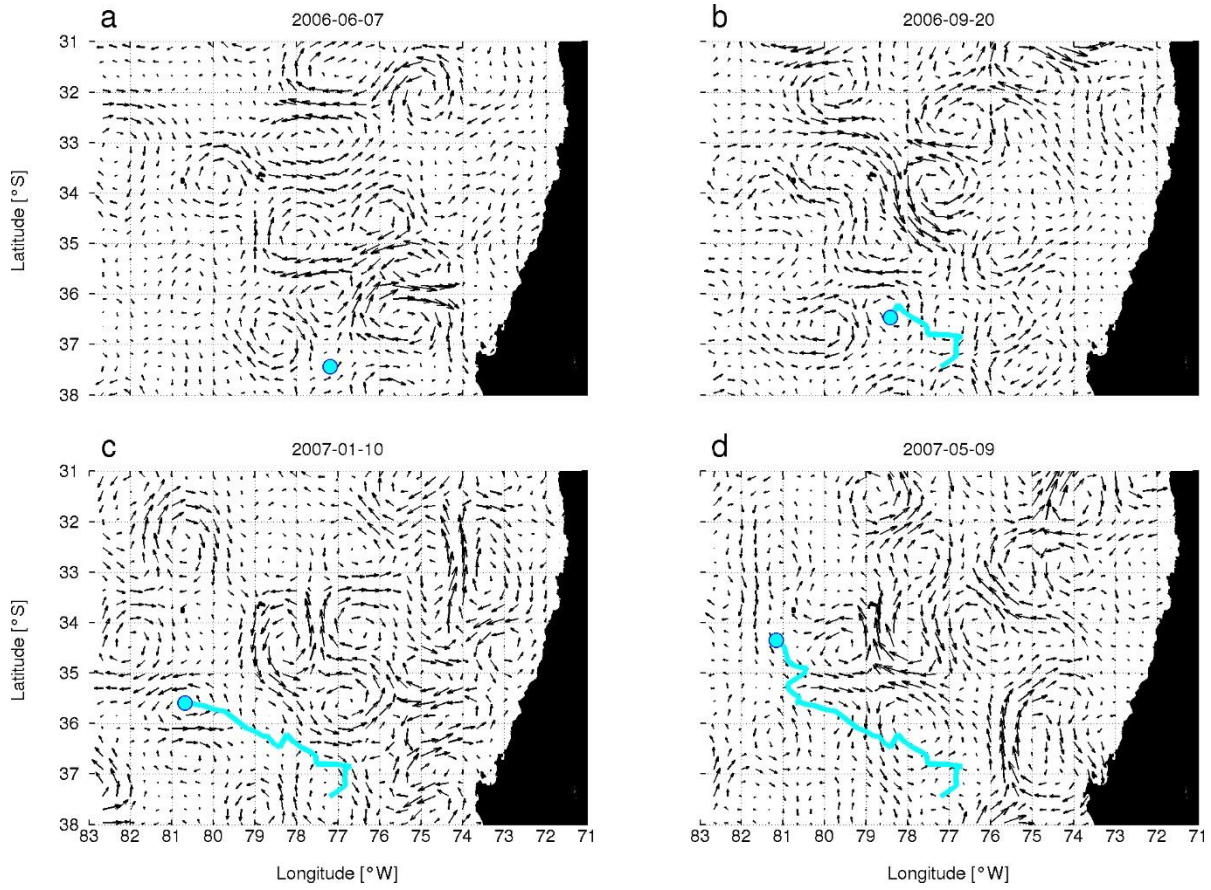

Figure 3. Four stages (a, b, c, d) of the ITE trajectory identified in the vertical sections of Figure 2 obtained during the research cruise of the corresponding BIP-2006 project. The arrows represent geostrophic current surface fields (cm s^{-1}) and the light blue lines represent the path of the eddy mass center. The light blue circles represent the eddy location for the date graphed.

within the CTZ (~35.8°S and ~74.5°W) during spring and reached the study region after 12 weeks (~80 days). The eddy moved ~120 km in a northwesterly direction with a mean velocity of ~1.4 km d^{-1} (Fig. 6b), slightly slower than what is typically reported for these eddies (~2 km d^{-1}). However, the speed of the eddy varies within its 65 weeks lifetime (1.2 years). We observed, for example, that its speed significantly reduced when it crossed the JFA. In fact, its interaction with the JFA takes place for several weeks during the eddy's trajectory, with the longest interaction time occurring with the RC-SC islands (9 weeks; June-July 2003).

To assess the importance of ITEs on the JFA productivity, we follow the evolution of satellite chlorophyll-a along the path of the eddy described above.

Fields of surface Chl-*a*, together with the geostrophic current derived from satellite altimetry data during June-July 2003 are shown in Figure 7. A closer inspection of the eddy evolution during June-July 2003 shows that its shape changes when it encounters the JFA bathymetry features (similar to the previous modeled eddy). We notice that it takes ~1 month for the chlorophyll concentration to respond to the presence of the eddy, reaching Chl-*a* concentrations up to 0.4 mg m^{-3}. At the end of the analyzed period (end of July 2003), the bloom of chlorophyll was maximum (0.4-0.5 mg m^{-3}).

Variability of model ITEs

To evaluate the variability of model ITEs, we choose to analyze the model depth of the 8° and 11°C isotherms during the period 2000-2007. The 8° and 11°C isotherms present the highest depression in the base and upper limit (near the seasonal thermocline) of ITEs R1 and R2 (Fig. 4). The vertical fluctuations of the 11°C isotherm should therefore reflect the disturbances associated with both the passage of Rossby waves and ITEs, while the variability of 8°C isotherm should better represent the fluctuations associated with the

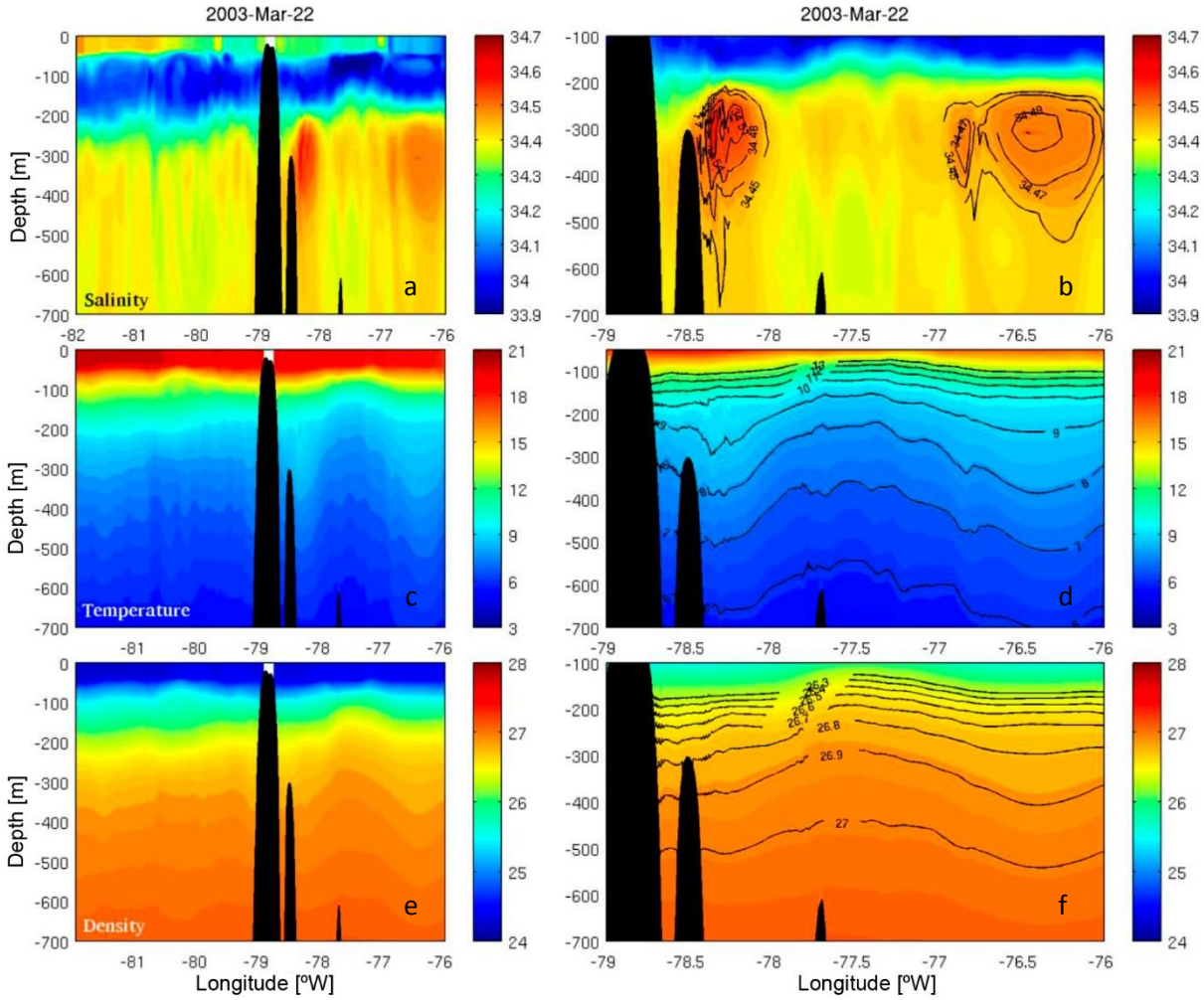

Figure 4. Vertical distribution (0-700 m depth) of a-b) salinity, c-d) temperature (°C), and e-f) density (sigma-t) around the RC-SC islands for the date 2003-03-22. The left panels show the section at 33.64°S and between 76°-82°W, and the right panels show a magnified view of two ITEs identified between 76°-79°W.

passage of ITEs. Thus, based on the behavior of the 8° and 11°C isotherms depth, one can differentiate between the disturbance generated by the presence of ITE and Rossby waves.

The spatial and temporal variability of fluctuations in the depths of the 8°C (Z8) and 11°C (Z11) isotherms for the 2000-2007 period were analyzed using the MTM-SVD method. The local fractional variance spectra obtained with the MTM-SVD method for Z8 and Z11 are shown in Figure 8. The Z8 spectrum (Fig. 8a) present significant variance in the 7 and 4.3 years periods, which are usually associated with large-scale processes such as El Niño Southern Oscillation (Correa-Ramírez *et al.,* 2012). Within the semiannual and seasonal bands, significant fluctuations are observed at periods of ~195 days (>95%) and ~127 days (>80%), respectively. These fluctuations might be linked to mesoscale variability present in the study region. Considering that Z8 is located at an average depth of ~400 m, it suggest that annual scale processes do not have any great impact at mesobatic depths.

The spectrum of Z11 showed significant values at interannual, annual, semi-annual and seasonal frequencies (Fig. 8b). Fluctuations in the low-frequency band (~7 and ~3 years) are generally associated with large-scale processes such as El Niño Southern Oscillation (Correa-Ramírez *et al.,* 2012). Unlike the Z8 depth, the Z11 depth exhibits energy maxima at 1 year and ~288 days. In general, the increase of energy at these frequency bands has been associated with Rossby wave propagation (Chelton & Schlax, 1996; Correa-Ramírez *et al.,* 2012). Similar

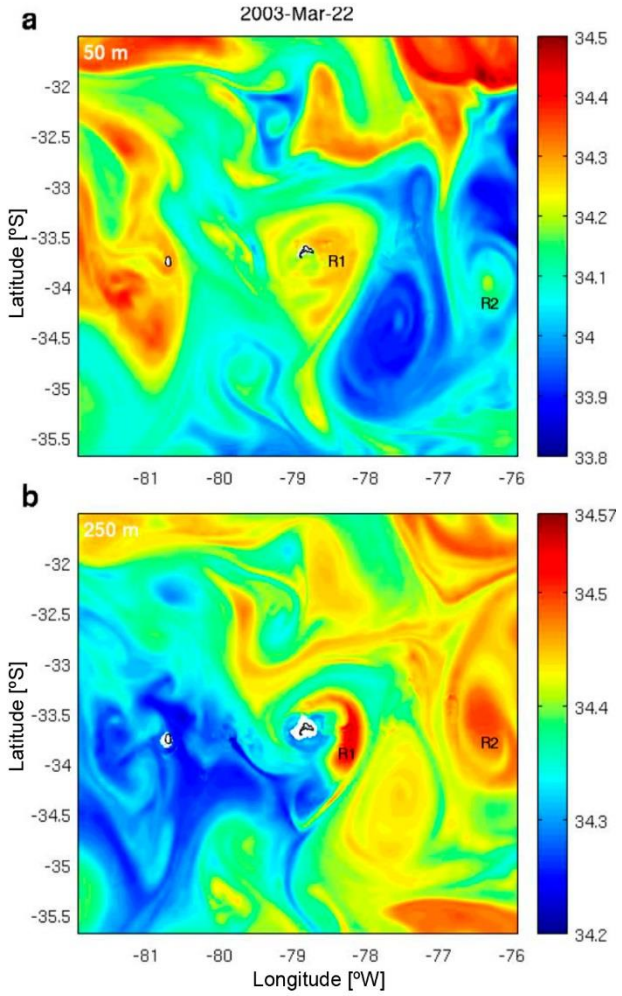

Figure 5. Salinity fields, obtained with ROMS, for one horizontal section at a) 50 m, and b) 250 m depth for the date 2003-03-22 in the region between 31°-36°S and 76°-82°W. R1 and R2 are the ITEs selected for analysis.

to the Z8 spectrum, significant frequencies are found in the semiannual (~193) and seasonal (~126) band, which suggests that the disturbances observed in Z8 and Z11 correspond to a disturbance covering several hundred meters in the water column and could be related to mesoscale variability generated by ITEs.

Space reconstruction

Because the Z8 and Z11 local fractional variance spectra (Fig. 8) share a significant maximum in the semiannual and seasonal bands with a similar period (195 and 127 days), the respective frequencies were reconstructed to evaluate whether these fluctuations are associated with mesoscale variability generated by ITEs.

The spatial reconstruction of the anomalies in Z8 frequency corresponding to the 195 days period calculated through the MTM-SVD method for the 2000-2007 time series is shown in Figure 9. The 195 day period represents 4.6% of the total variance in the region. The zero phase of the cycle corresponds to the start date of the series (2000-07-17), the 315 phase corresponds to 171 days later, and the 360 phase to 195 days after the start date of the time series, therefore by each year 1.8 cycles are produced. The negative (positive) anomalies represent a higher (lower) depth of the 8°C isotherm. The figure shows that disturbance of the isotherm depth presents closed structures of an elongated oval shape that spread from the southeast to the northwest of the study region. Propagation towards the northwest indicates a non-linear signal, differing from the linear Rossby wave propagation in these latitudes (Chelton *et al.,* 2007). Moreover, it was observed that the structures presented a propagation speed slightly higher than the theoretical propagation speed for the first baroclinic mode of a Rossby wave (gray dashed line). Furthermore, the horizontal spatial scale associated with these structures had a greater size than expected for Rossby waves. In general, the features described for the figure suggest that these structures are not Rossby waves. When those structures interact with the RC-SC islands (45 and 90 phases), a slight increase in speed is observed (Fig. 9), which may correspond to an effect of the ridge on the incident flows. In addition, it was observed that the islands have a different impact on the propagation of the structures. While the RC-SC islands generate increased speed in propagation towards the northwest, the AS island diverts the trajectory of the structures slightly to the south (180, 225 and 270 phases), without affect significantly their velocity.

Figure 10 shows the spatial reconstruction of the Z11 anomalies in the frequency corresponding to the 193 days period calculated through the MTM-SVD method for the time series between 2000-2007. The variance for the 193 days period represents 4.7% of the total variance in the region. The zero phase of the cycle corresponds to the start date of the series (2000-01-17), the 315 phase corresponds to 169 days later, and the 360 phase to 193 days later, therefore, each year contains 1.9 cycles. The negative (positive) anomalies represent a higher (lower) depth of the 11°C isotherm. In this figure we note that Z11 fluctuations present a spatial structure similar to Z8 (Fig. 10), with the same propagation pattern from southeast to northwest. The structures in Z11 are slightly smaller in relation to those observed in Z8, suggesting that they represent the most superficial fraction of a process developed at a greater depth. The features observed in both reconstructions allow the dismissal of the idea that the observed fluctuations in this frequency band correspond to Rossby waves coinciding with those expected for ITEs

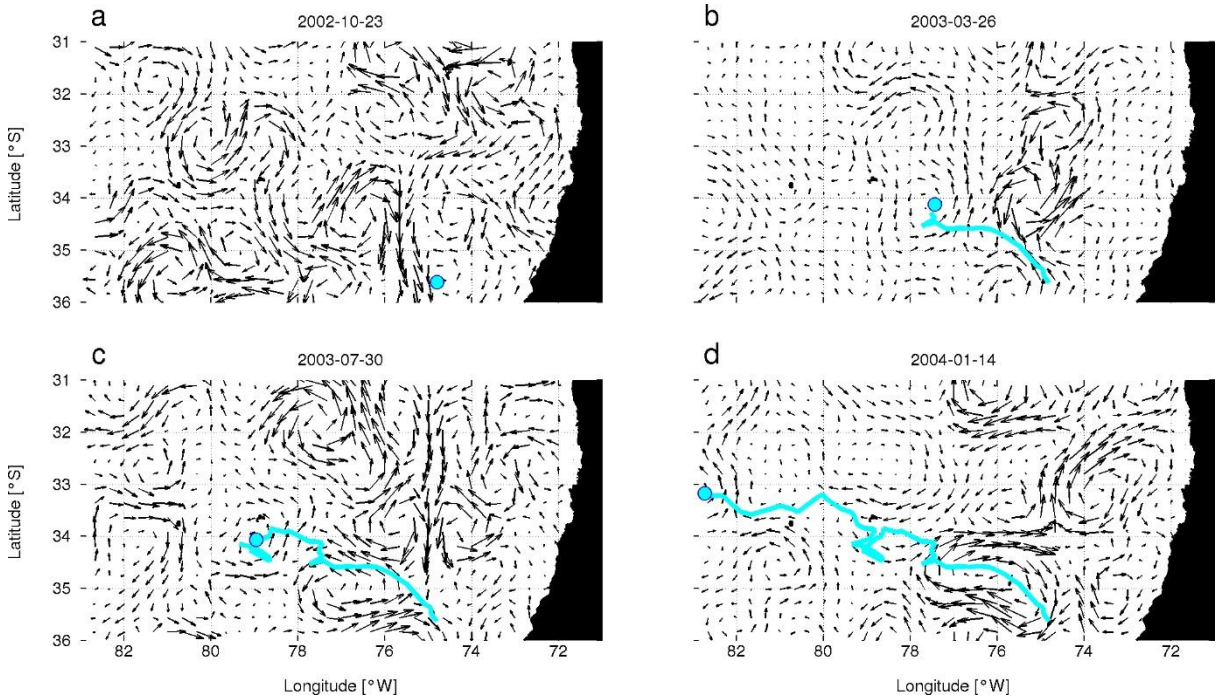

Figure 6. Four stages (a, b, c, d) of the ITE trajectory formed in the continental coastal zone. The arrows represent the surface field of geostrophic currents (cm s^{-1}) obtained by satellite altimetry and the light blue lines represent the path of the eddy mass center through the Okubo-Weiss parameter. The light blue circles represent the eddy location for the date graphed.

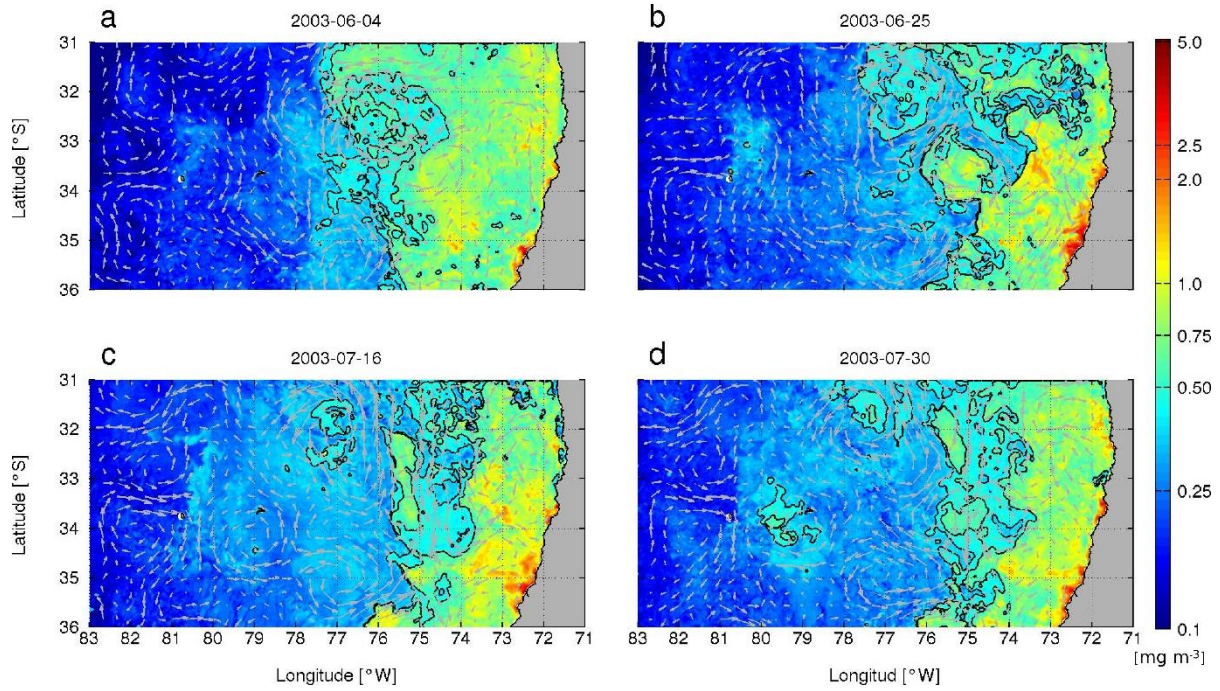

Figure 7. Chlorophyll-*a* fields (color, mg m^{-3}) superimposed on the surface field of geostrophic current (cm s^{-1}) for the period in which the interaction of an anticyclonic eddy (identified by satellite, Fig. 6) is observed with the JFA. The contours are chlorophyll-*a* isolines of 0.4 and 0.5 mg m^{-3}.

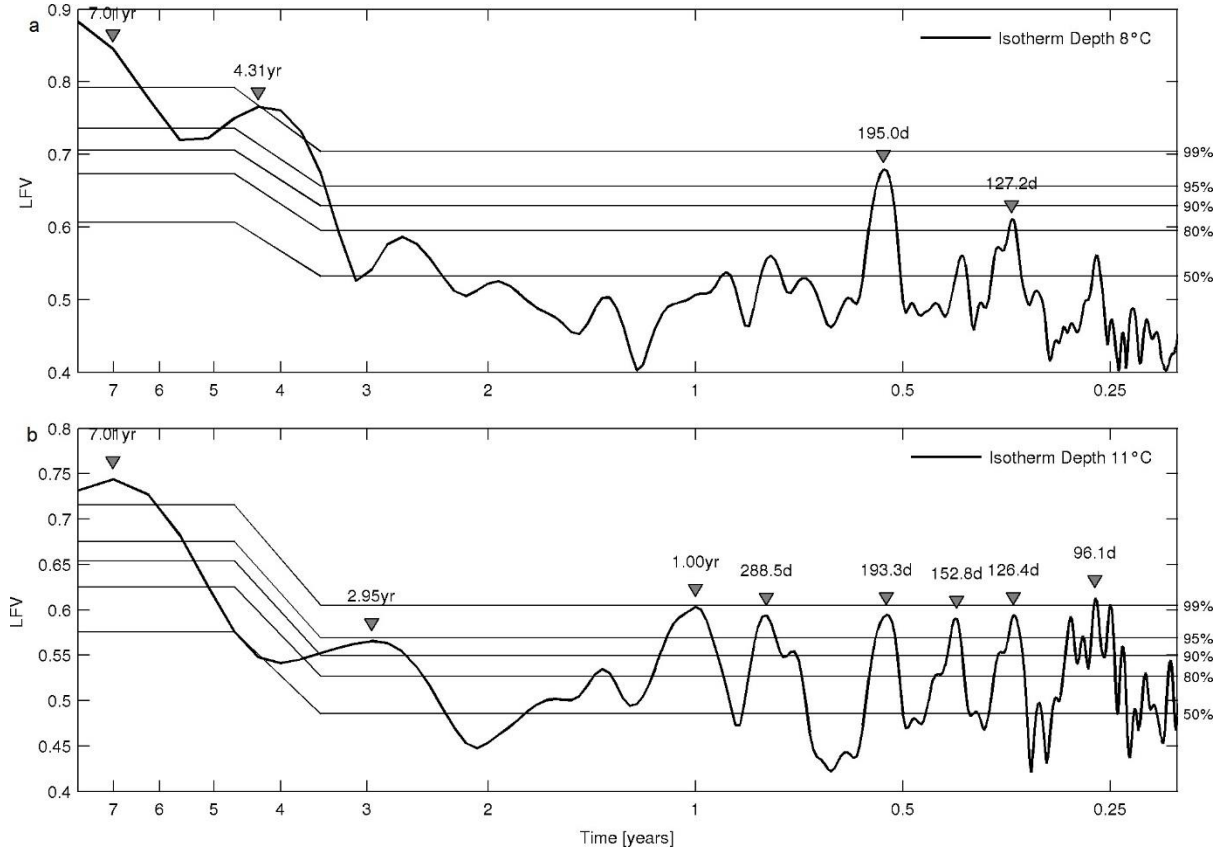

Figure 8. Local fractional variance spectra (LFV)greater than the seasonal frequency (period >0.25) for a) depth of the 8°C isotherm (Z8), and b) depth of the 11°C isotherm (Z11). Confidence levels used are 50%, 80%, 90%, 95%, 99%, which were calculated by a random resampling experiment.

(Johnson & McTaggart, 2010; Colas *et al.,* 2011; Hormazábal *et al.,* 2013).

Figure 11 shows the spatial reconstruction of the Z8 anomalies for the corresponding ~126 day period frequency, calculated by the MTM-SVD method for the time series between 2000-2007. For this frequency, the variance represents 2.5% of the total variance in the region. The zero phase of the cycle corresponds to the start date of the series (2000-01-17), the 315 phase corresponds to 111 days later, and the 360 phase to 126 days later, therefore by each year 2.87 cycles are produced. The negative (positive) anomalies represent a higher (lower) depth of the 8°C isotherm, where the negative anomalies correspond to the lower limit deflection of the thermocline with a concave shape. Due to the displacement velocity and the size of the eddies this frequency has been associated with the time that it takes an eddy to pass a fixed point (Hormazábal *et al.,* 2004). The figure shows that the maximum (minimum) amplitude of the signal propagates from southeast to northwest. A train of latitudinal aligned structures was observed east of the JFA (E1a, E2a, E3a; phase zero). This type of alignment had been observed previously in Iberian basins and the Canary Islands (Meddies; Richardson *et al.,* 2000) and, more recently, for the eastern boundary system of Chile-Perú (Hormazábal *et al.,* 2013). For the next phase (45 phase), the union of both upper structures (E1a and E2a) located north of the archipelago was assessed. This union seems to be promoted by a slight increase in the velocity of the structures as they go across the ridge axis. However because the displacement of these structures is slow, the interaction period between them and the islands (set RC-SC: 315, 0 and 45 phases; AS island: 135, 180 and 225 phases) can last ~42 days (~1.4 months).

Figure 12 shows the Z11 spatial reconstruction, for the frequency corresponding to the 126 days period calculated through the MTM-SVD method for the 2000-2007 time series. The 126 days period variance represents 2.75% of the total variance of the region. The zero phase of the cycle corresponds to the start date of the series (2000-01-17), the 315 phase corresponds to 110 days later, and the 360 phase to 126 days later,the-

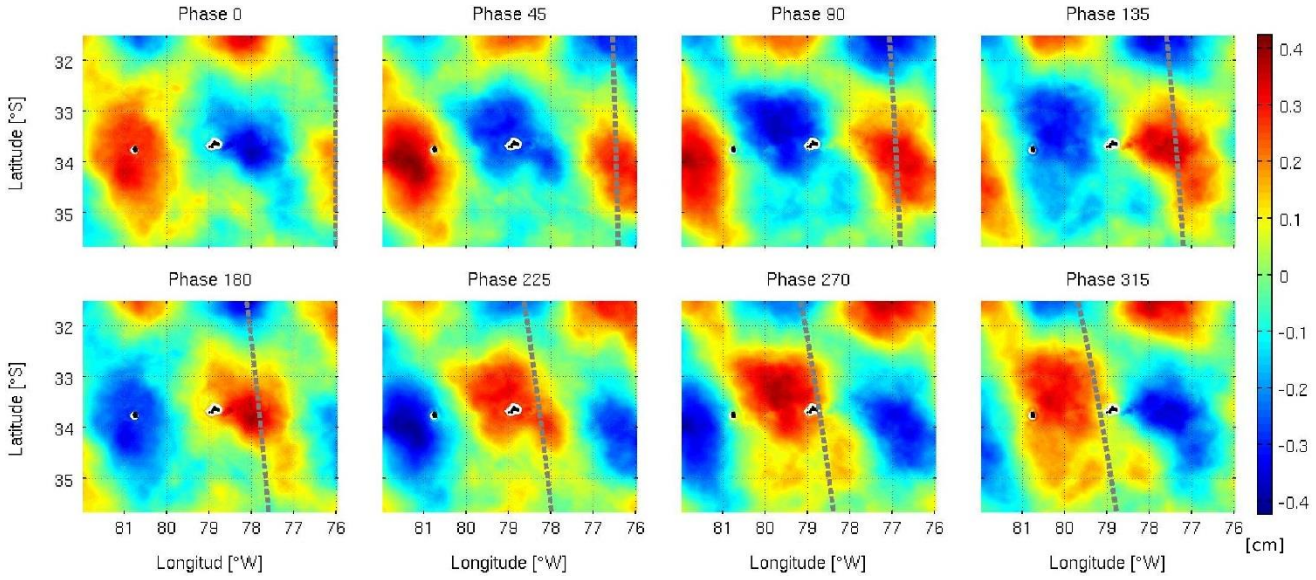

Figure 9. Spatial reconstruction of depth anomalies for the 8°C isotherm (Z8) for the 195 days period obtained through the MTM-SVD method. Each frame is 45°. The zero phase of the cycle corresponds to the start date of the series (2000-01-17), phase 315 corresponds to 171 days after, and phase 360 to 195 days after. 1.8 cycles occur per year. The gray dashed line corresponds to the theoretical speed of propagation of a first baroclinic mode of a Rossby wave (Chelton *et al.,* 1998).

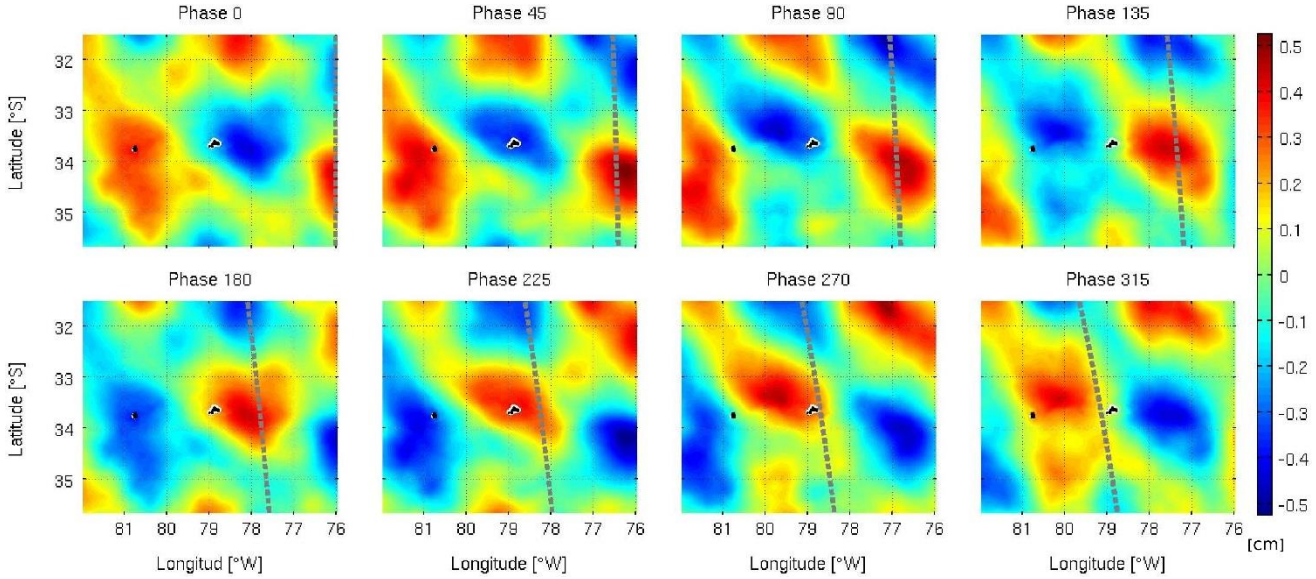

Figure 10. Depth anomaly spatial reconstruction for the 11°C isotherm (Z11) for the 193 days period obtained through the MTM-SVD method. Each frame is 45°. The zero phase of the cycle corresponds to the start date of the series (2000-01-17), phase 315 corresponds to 169 days after, and phase 360 to 195 days after. 1.9 cycles occur per year. The gray dashed line corresponds to the theoretical propagation speed of a first baroclinic mode of a Rossby wave (Chelton *et al.,* 1998).

refore 2.89 cycles are produced each year. The positive (negative) anomalies represent a lower (higher) depth for the 11°C isotherm. A propagation pattern that differs slightly from that presented in Figure 11 was observed. The maximum (minimum) signal amplitude spreads from southeast to northwest under below the ridge axis of the JFA, and from east to west over the ridge axis, suggesting that the western fraction of the ridge (82°-76°W) represents a physical barrier for the incident flow. Similar to the Z8 reconstruction (Fig. 11), at the zero phase a train of structures (E1b, E2b, E3b) at the east of the archipelago are observed, but in opposite phase, which means that in this isotherm the deflection is represented as a convex form in the upper limit of the

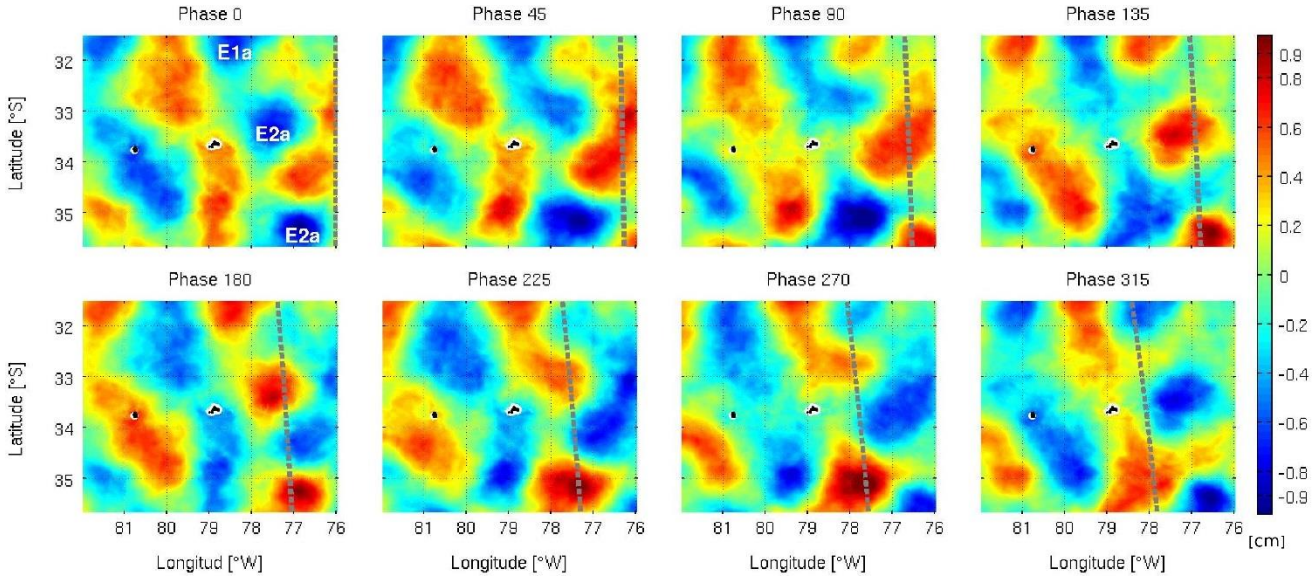

Figure 11. Depth anomaly spatial reconstruction for the 8°C isotherm (Z8) for a 127 days period of obtained through the MTM-SVD method. Each frame is 45°. The zero phase of the cycle corresponds to the start date of the series (2000-01-17), phase 315 corresponds to 111 days after, and the phase 360 to 127 days after. 2.87 cycles occur per year. The gray dashed line corresponds to the theoretical speed of propagation of a first baroclinic mode of a Rossby wave (Chelton *et al.,* 1998).

thermocline, reinforcing the idea that the observed structures correspond to ITEs. Nevertheless, the convex deflection shape of the 11°C isotherm is not observed for those structures located south of the Juan Fernández ridge axis (E3b). This might be associated to a latitudinal difference in the stratification on top of the water column or the presence of another forcing that operates on the same frequency. Moreover, the propagation of the Z11 structure, relative to that observed with Z8, presents less interaction with the islands that form the archipelago where the interaction with the AS island is the most intense.

DISCUSSION

The results of this study revealed the presence of long-life (≥1 year) and weak surface expression ITEs interacting with the topography of the JFA with a semiannual frequency, mainly in the austral autumn period. This agrees with what was described by Morales *et al.* (2012) and Hormazábal *et al.* (2013), who observed the formation of ITEs in the CTZ ~6 months before arriving at the JFA, mainly during spring-summer periods when intensified coastal upwelling occurs. Model results show the eddies' simultaneous occurrence in time, which is supported by observations in other oceanic regions (Richardson *et al.,* 2000), and recently in the coastal zone off central Chile (Hormazábal *et al.,* 2013).

The ITES were initially identified in the CTZ (Figs. 4-7). The trajectories presented slightly lower propagation velocities (~1.16 and ~1.4 km d^{-1}) than those previously reported (~2 km d^{-1}; Hormazábal *et al.,* 2013), which in some cases could delay the arrival of these eddies to JFA until winter.

The depth fluctuation analysis of the 8°C (Z8) and 11°C (Z11) isotherms revealed the presence of significant fluctuations with periods of ~190 and ~120 days, which are mainly associated with mesoscale eddies because they do not present a linear propagation. Rather, they have a slightly higher propagation velocity than the first baroclinic mode of a Rossby wave and are larger than the internal radius of Rossby deformations for the region (~25-30 km; Chelton *et al.,* 1998). According to the time scale for coastal trapped disturbances, periods ~180 days should be restrained to the coast; however; the spatial reconstruction of Z8 and Z11 for the ~190 day period agree with a non-linear propagation of eddies. The current fluctuations with periods of ~120 days have been associated with mesoscale eddies (Hormazábal *et al.,* 2004). The spatial reconstruction of Z8 and Z11 in the ~120 day period presented a convex deflection shape in the upper limit of the eddy at Z11, and a concave shape at Z8, which coincides with the expected vertical structure for an ITE.

Due to the northwestern propagation direction of the eddies, it was observed that the surface and subsurface

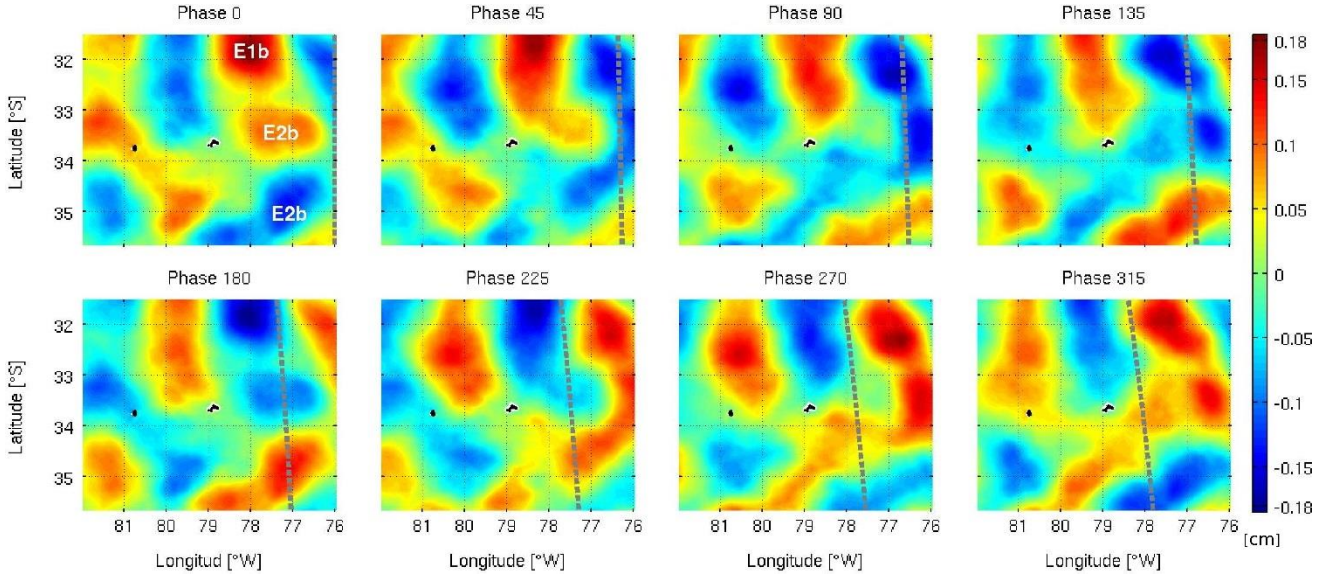

Figure 12. Spatial reconstruction of the depth anomalies for the 11°C isotherm (Z11) for a of 126 days period obtained through the MTM-SVD method. Each frame is 45°. The zero phase of the cycle corresponds to the start date of the series (2000-01-17), phase 315 corresponds to 110 days after, and phase 360 to 126 days after. 2.89 cycles occur per year. The gray dashed line corresponds to the theoretical speed of propagation of a first baroclinic mode of a Rossby wave (Chelton *et al.,* 1998).

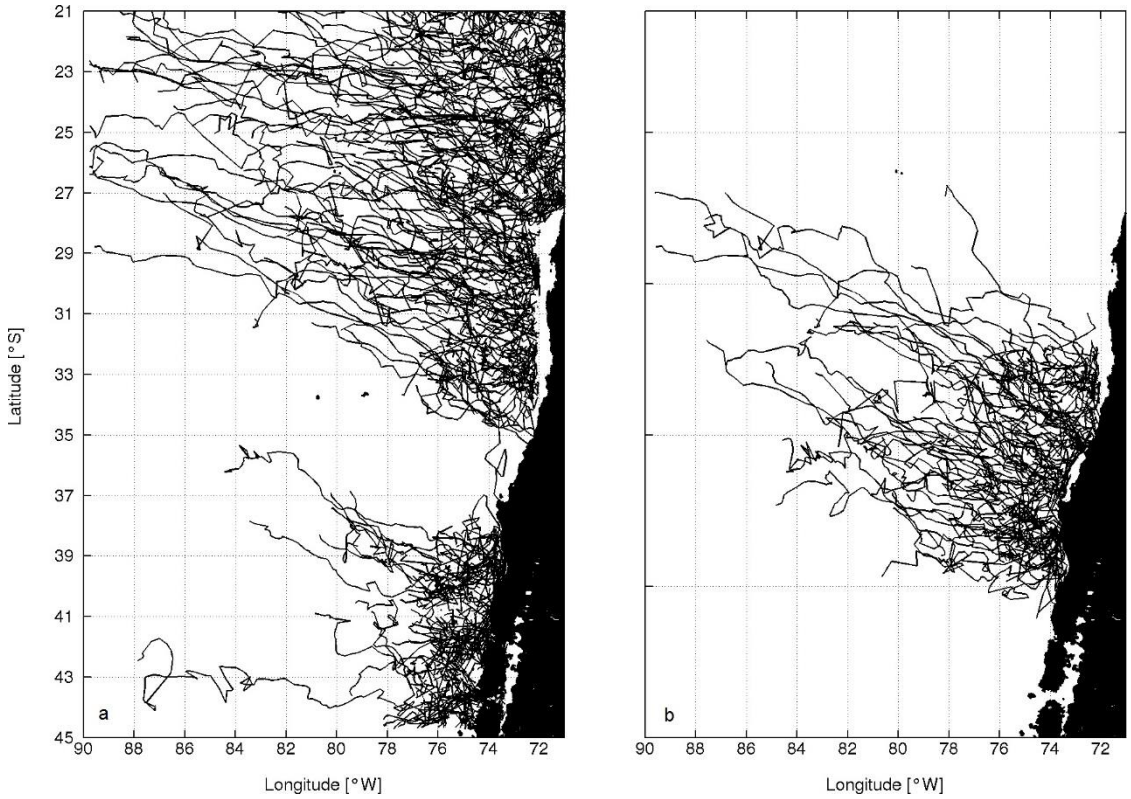

Figure 13. Anticyclonic eddy trajectories identified with satellite altimetry between longitudes 71°-76°W for three latitudinal sections: a) 21°-33°S (upper part), 39°-45°S (lower part), and b) 33°-39°S.

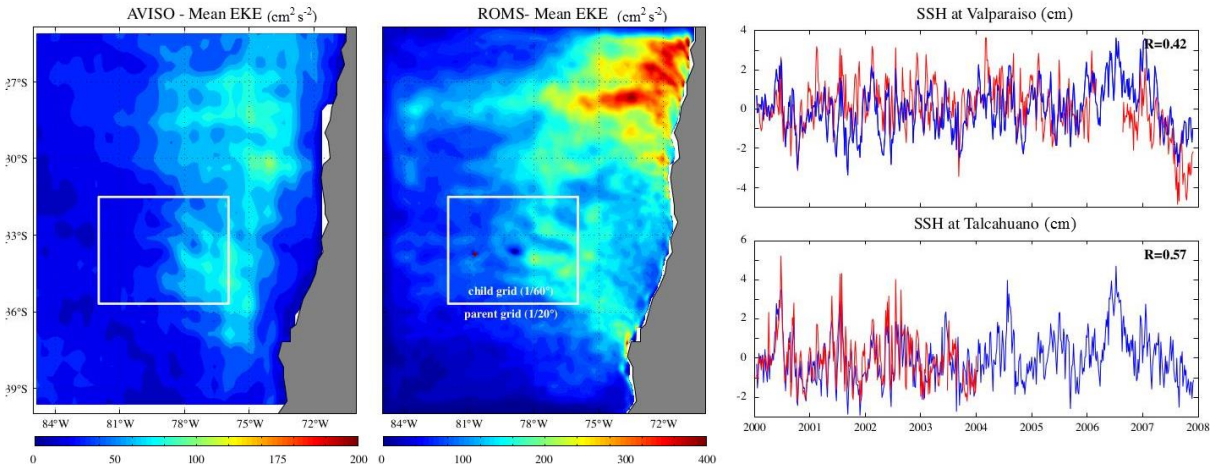

Figure A1. a) Mean satellite surface EKE, b) mean model EKE in ($cm^2\ s^{-2}$), and c) compares the model (blue) and *in situ* (red) Sea Surface Height at Valparaíso and Talcahuano.

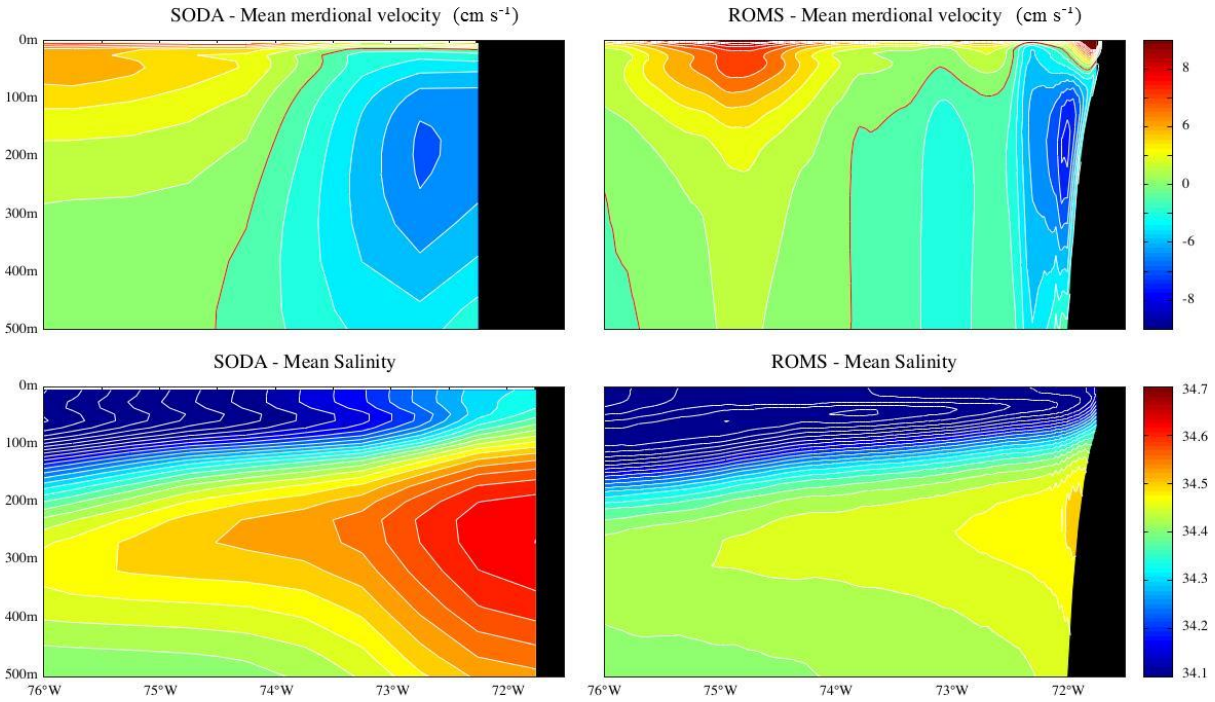

Figure A2. The first row compares the mean meridional velocity from ROMS and SODA at 33.25°S in cm s^{-1}. The contour interval is 1 cm s^{-1}. Red contour indicates the 0 cm s^{-1} contour. Second row compares the mean salinity from ROMS and SODA at 33.25°S. The salinity of contour interval is 0.025.

anticyclonic structures that interact with the JFA originated mainly from the coastal band between 33° and 39°S, as shown in Figure 13. This result, obtained from eddy trajectories followed by satellite altimetry, defines the geographic area of the continental edge that interacts with the JFA through mesoscale variability.

Based on satellite altimetry data and oceanographic cruises, it was observed that ITEs have a weaker surface expression with respect to adjacent surface eddies. In some cases, these eddies may present a surface expression with the shape of bi-convex lenses (Fig. 7a) since their vertical coherence causes a deformation at the upper water column (Filyushkin *et al.,* 2011b). It has been documented that the interaction of ITEs with seamounts may also destroy them totally or partially (*e.g.,* Meddies; Filyushkin *et al.,* 2011a). In the first

case, total destruction might generate additional water mixing mechanisms in the intermediate layers, and in the second case, eddy fragments may stay on topographical elevations for long periods of time (Filyushkin *et al.,* 2011a).

As ITEs, retain much of the physical and chemical characteristics of water masses acquired in their formation zone during displacement westward (Nauwn *et al.,* 2006; Johnson & McTaggart, 2010), which in the southeastern Pacific Ocean are associated with ESSW, they should play an important role in the transport of nutrients to oligotrophic waters, as has been observed for mesoscale eddies in other eastern boundary systems (*e.g.,* Gruber *et al.,* 2011). Thus, the ITEs observed off Chile should produce significant effects on the dynamics of pelagic biological systems throughout their trajectory, as well as during their interaction with the islands and seamounts present in this oceanic region.

Chl-*a* satellite fields overlapped on the current satellite fields, showed significant surface increases in Chl-*a* associated with anticyclonic eddies of weak surface expressions (Fig. 7). It is probable that these increases are the maximum surface expression developed below the surface, as reported for ITEs in other oceanic regions (McGillicuddy *et al.,* 2007; Kim *et al.,* 2011). In the JFA, high surface Chl-*a* concentrations have been detected reaching values of ~2 mg m^{-3} in AS island and ~1 mg m^{-3} in the RC-SC islands (Pizarro *et al.,* 2006). Thus, the exclusive use of satellite data to evaluate Chl-*a* concentrations associated with mesoscale eddies would underestimate the real impact of these structures on biological production in the region. The mechanism behind these increases is unknown. In this sense, the meso and submesoscale structures may play an important role in the increases in biological production.

It has been observed that the composition of phytoplankton inside the ITEs is dominated by phytoplankton classes of large size (>20 μm), mostly diatoms, as in the ITEs of northwest Atlantic Ocean (mode-water eddy; McGillicuddy *et al.,* 2007), the East Sea of Japan (UWE; Kim *et al.,* 2011) and the Sea of Norway (Hansen *et al.,* 2010). However, in the southeastern Pacific ITEs, a predominance of smaller phytoplankton: nanophytoplankton (between 20-3 μm in diameter) has been observed (Morales *et al.,* 2012). Since picoplankton species (<2-3 μm in diameter) dominate meso-oligotrophic regions, (*e.g.,* region JFA; Stockner, 1988; Grob *et al.,* 2007), collecting samples *in situ* in these waters is essential to evaluate the impact of ITEs on smaller groups of phytoplankton as well as the subsequent transfer of energy to higher trophic levels.

Based on the analysis of ROMS model results, two ITEs (R1 and R2) were identified interacting with JFA islands during the austral autumn (Fig. 4). As result of this interaction, a horizontal/vertical deformation (narrowing/expansion) of the eddy favoring the isolines eddy elevations within the euphotic zone (Fig. 5), which would act as an injection mechanism of nutrients from ESSW necessary to generate increases in phytoplankton around the islands, was observed. Although the model did not consider data assimilation, through the combined use of these and satellite information, it was possible to identify an anticyclonic eddy of weak surface expression interacting with the JFA. The interaction between the eddy and the RC-SC islands took place over a nine-week period that included the autumn-winter transition period (Fig. 7). Increases in satellite Chl-*a* concentrations were observed a month after the start of the interaction (winter), with values up to three times higher with respect to adjacent oceanic waters, reinforcing the idea of importance of mesoscale eddies on temporal and spatial Chl-*a* satellite variability in this insular system of the southeastern Pacific.

Appendix A

Throughout this section, we provide a qualitative comparison of the general circulation between the model solution and observations. To assess the model's ability to reproduce the eddy activity, we compare the model mean Eddy Kinetic Energy (EKE) with the one derived from AVISO altimetry (Figs. A1a, A1b). Both mean EKE are computed from sea surface height (SSH) for the period 2000-2007. Although the model strongly overestimates the satellite mean EKE, the spatial structure shows a good agreement, in particular off central Chile. Both show maximum values west of 75W with minimum EKE along the coast. The coastal SSH variability, which strongly depends on the wind stress variability and propagating signals from the equator also shows good agreement with in-situ observation (provided by the University of Hawaii Sea Level Center http://ilikai.soest.hawaii.edu/uhslc/data.html; Fig. A1c).

We have shown that the model also reasonably reproduced the structure of individual ITEs originating in the PCUC (Figs. 2-4). Figure A2 compares the vertical structure of the model and observed (SODA) PCUC at 33°S. Both, the mean meridional velocity and mean salinity agree well with observed values. However, the model PCUC salinity underestimates the observed one (~0.125 difference). This may be due to an underestimation of the salinity imposed at the northern boundary. Note, however, that the individual ITE exhibits similar salinity values compared to the observed ITEs salinity (Fig. 4).

ACKNOWLEDGMENTS

This study was supported by the "Fondo Nacional de Ciencia y Tecnología" (FONDECYT) Project N°1131047 (S. Hormazábal). I. Andrade was funded by a doctoral scholarship from the Pontificia Universidad Católica de Valparaíso. The authors thank the Ocean Biology Processing Group (Code 614.2) at the Goddard Space Flight Center, Greenbelt, MD 20771, for the production and distribution of the ocean color data. The comments of anonymous reviewers were very helpful.

REFERENCES

Alvera-Azcárate, A., A. Barth, M. Rixen & J.M. Beckers. 2005. Reconstruction of incomplete oceanographic data sets using empirical orthogonal functions. Application to the Adriatic Sea surface temperature. Ocean Model., 9: 325-346.

Alvera-Azcárate, A., A. Barth, J.M. Beckers & R.H. Weisberg. 2007. Multivariate reconstruction of missing data in sea surface temperature, chlorophyll, and wind satellite fields. J. Geophys. Res-Oce, 112, C03008. doi:10.1029/2006JC003660.

Amante, C. & B.W. Eakins. 2009. ETOPO1 1 Arc-Minute Global Relief Model: procedures, Data sources and analysis. NOAA Technical Memorandum NESDIS NGDC-24, 19 pp.

An, H.S., K.S. Shim & H.R. Shin. 1994. On the warm eddies in the southwestern part of the East Sea (the Japan Sea). J. Korean Soc. Oceanogr., 29: 152-163.

Andrade, I., S.E. Hormazábal & M.A. Correa-Ramírez. 2012. Ciclo anual de la clorofila-*a* satelital en el archipiélago Juan Fernández (33°S), Chile. Lat. Am. J. Aquat. Res., 40(3): 657-667.

Andrade, I., P. Sangrà, S.E. Hormazábal & M.A. Correa-Ramírez. 2014. Island mass effect in the Juan Fernández Archipelago (33°S), Southeastern Pacific. Deep-Sea Res. I, 84: 86-99.

Aristegui, J., P. Tett, A. Hernández-Guerra, G. Basterretxea, M.F. Montero, K Wild, P. Sangrà, S. Hernández-León, M. Canton, J.A. García-Braun, M. Pacheco & E.D. Barton. 1997. The influence of island-generated eddies on chlorophyll distribution: a study of mesoscale variation around Gran Canaria. Deep-Sea Res. I, 44(1):71–96.

Armi, L. & W. Zenk. 1984. Large lenses of highly saline Mediterranean water. J. Phys. Oceanogr., 14: 1560-1576.

Bakun, A. 2006. Fronts and eddies as key structures in the habitat of marine fish larvae: opportunity, adaptive response and competitive advantage. Sci. Mar., 70(S2): 105-122.

Beckers, J.M. & M. Rixen. 2003. EOF calculations and data filling from incomplete oceanographic data sets. J. Atmos. Ocean. Technol., 20(12): 1839-1856.

Chaigneau, A., M. Le Texier, G. Eldin, C. Grados & O. Pizarro. 2011. Vertical structure of mesoscale eddies in the eastern South Pacific Ocean: a composite analysis from altimetry and Argo profiling floats, J. Geophys. Res. Oceans, 116, C11025, doi:10.1029/2011JC 007134.

Chelton, D.B. & M.G. Schlax. 1996. Global observations of oceanic Rossby waves. Science, 272: 234-238.

Chelton, D.B., M.G. Schlax, R.M. Samelson & R.A. de Szoeke. 2007. Global observations of large ocean eddies. Geophys. Res. Lett., 34, L15606, doi:10.1029/2007GL030812.

Chelton, D.B., R.A. deSzoeke, M.G. Schlax, K. El Naggar & N. Siwertz. 1998. Geographical variability of the first-baroclinic Rossby radius of deformation. J. Phys. Oceanogr. 28: 433-460.

Colas, F., J. McWilliams, X. Capet & J. Kurian. 2011. Heat balance and eddies in the Peru-Chile Current System, Clim. Dynam., 39(1): 509-529.

Correa-Ramírez, M. & S. Hormazábal. 2012. MultiTaper Method-Singular Value Decomposition (MTM-SVD): variabilidad espacio-frecuencia de las fluctuaciones del nivel del mar en el Pacífico suroriental. Lat. Am. J. Aquat. Res., 40(4): 1039-1060.

Correa-Ramírez, M.A., S. Hormazábal & G. Yuras. 2007. Mesoscale eddies and high chlorophyll concentrations off central Chile (29°S-39°S). Geophys. Res. Lett., 34, L12604.

Correa-Ramírez, M.A., S.E. Hormazábal & C.E. Morales. 2012. Spatial patterns of annual and interannual surface chlorophyll-*a* variability in the Perú-Chile system. Prog. Oceanogr., 92-95: 8-17.

Da Silva, A.M., C.C. Young & S. Levitus. 1994. Atlas of surface marine data 1994, Vol. 1, algorithms and procedures, NOAA Atlas NESDIS 6, U.S. Department of Commerce, NOAA, NESDIS, USA, 74 pp.

Debreu, L., P. Marchesiello, P. Penven & G. Cambon. 2011. Two-way nesting in split-explicit ocean models: algorithms, implementation and validation. Ocean Model., 49-50: 1-21.

Doty, M.S. & M. Ogury. 1956. The island mass effect. J. Cons. Int. Explor. Mer., 22: 33-37.

Dugan, J.P., R.P. Mied, P.C. Mignerey & A.F. Schuetz. 1982. Compact, intrathermocline eddies in the Sargasso Sea, J. Geophys. Res., 87(C1): 385-393.

Falkowski, P.G., D. Ziemann, Z. Kolber & P.K. Bienfang. 1991. Role of eddy pumping in enhancing primary production in the ocean. Nature, 352(6330): 55-58.

Filyushkin, B.N., M.A. Sokolovskiy, N.G. Kozhelupova & I.M. Vagina. 2011a. Evolution of intrathermocline eddies moving over a submarine hill. Doklady Earth Sci., 441(2): 1757-1760.

Filyushkin, B.N., M.A. Sokolovskiy, N.G. Kozhelupova & I.M. Vagina. 2011b. Reflection of intrathermocline eddies on the ocean surface. Doklady Earth Sci., 439(1): 118-121.

Garfield, N., C.A. Collins, R.G. Paquette & E. Carter. 1999. Lagrangian exploration of the California Undercurrent, 1992-95. J. Phys. Oceanogr., 29: 560-583.

González-Ferrán, O. 1987. Evolución geológica de las Islas chilenas en el océano Pacífico. In: J.C. Castilla (ed.). Islas oceánicas chilenas: conocimiento científico y necesidades de investigación. Ediciones Universidad Católica de Chile, Santiago, pp. 37-54.

Gordon, A.L., C.F. Giulivi, C.M. Lee, H.H. Furey, A. Bower & L. Talley. 2002. Japan/East Sea intrathermocline eddies, J. Phys. Oceanogr., 32(6): 1960-1974.

Grob, C., O. Ulloa, W.K.W. Li, G. Alarcón, M. Fukasawa & S. Watanabe. 2007. Picoplankton abundance and biomass across the eastern south Pacific Ocean along latitude 32.5°S. Mar. Ecol. Prog. Ser., 332: 53-62.

Gruber, N., Z. Lachkar, H. Frenzel, P. Marchesiello, M. Münnich, J.C. McWilliams, T. Nagai & G. K. Plattner. 2011. Eddy-induced reduction of biological production in eastern boundary upwelling systems, Nat. Geosci., 4(11): 787-792.

Hansen, C., E. Kvaleberg & A. Samuelsen. 2010. Anticyclonic eddies in the Norwegian Sea; their generation, evolution and impact on primary production, Deep-Sea Res. I, 57(9): 1079-1091, doi:10.1016/j.dsr.2010.05.013.

Hormazábal, S., G. Shaffer & O. Leth. 2004. Coastal transition zone off Chile. J. Geophys. Res., 109, C01021, doi:10.1029/2003JC001956.

Hormazábal, S., V. Combes, C.E. Morales, M.A. Correa-Ramírez, E. Di Lorenzo & S. Nuñez. 2013. Intrathermocline eddies in the coastal transition zone off central Chile (31-41°S). J. Geophys. Res. Oceans, 118: 1-11, doi:10.1002/jgrc.20337.

Isern-Fontanet, J., J. Font, E. Garcia-Ladona, M. Emelianov, C. Millot & I. Taupier-Letage. 2004. Spatial structure of anticyclonic eddies in the Algerian basin (Mediterranean Sea) analyzed using the Okubo-Weiss parameter, Deep-Sea Res. II, 51(25-26): 3009-3028.

Johnson, G.C. & K.E. McTaggart. 2010. Equatorial Pacific 13°C water eddies in the eastern subtropical south Pacific Ocean. J. Phys. Oceanogr., 40(1): 226-236, doi:10.1175/2009JPO4287.1.

Kim, D., E.J. Yang, K.H. Kim, C-W. Shin, J. Park, S. Yoo & J-H. Hyun. 2011. Impact of an anticyclonic eddy on the summer nutrient and chlorophyll *a* distributions in the Ulleung Basin, East Sea (Japan Sea). ICES J. Mar. Sci., 69: 23-29.

Landaeta, M.F. & L.R. Castro. 2004. Zonas de concentración de ictioplancton en el Archipiélago de Juan Fernández, Chile. Cienc. Tecnol. Mar, 27(2): 43-53.

Leth, O. & G. Shaffer. 2001. A numerical study of seasonal variability in the circulation off central Chile, J. Geophys. Res., 106: 22,229-22,248.

Marchesiello, P., J.C. McWilliams & A. Shchepetkin. 2001. Open boundary conditions for long-term integration of regional oceanic models. Ocean Model., 3: 1-20.

Masumoto, Y., H. Sasaki, T. Kagimoto, N. Komori, A. Ishida, Y. Sasai, T. Miyama, T. Motoi, H. Mitsudera, K. Takahashi, H. Sakuma & T. Yamagata. 2004. A fifty year eddy-resolving simulation of the World Ocean-preliminary outcomes of OFES (OGCM for the Earth simulator). J. Earth Simul., 1: 31-52.

McGillicuddy, D., A. Robinson, D. Siegel, H. Jannasch, R. Johnson, T. Dickey, J. McNeil, A. Michaels & A. Knap. 1998. Influence of mesoscale eddies on new production in the Sargasso Sea. Nature, 394: 263-266.

McGillicuddy, D.J., L.A. Anderson, N.R. Bates, T. Bibby, K.O. Buesseler, C.A. Carlson, C.S., Davis, C. Ewart, P.G. Falkowski, S.A. Goldthwait, D.A., Hansell, W.J. Jenkins, R. Johnson, V.K. Kosnyrev, J.R. Ledwell, Q.P. Li, D.A. Siegel & D.K. Steinberg. 2007. Eddy/wind interactions stimulate extraordinary mid-ocean plankton bloom. Science, 316(5827): 1021-1026.

Mann, M.E. & J. Park. 1999. Oscillatory spatiotemporal signal detection in climate studies: a multiple-taper spectral domain approach. Adv. Geophys., 41: 1-131.

Morales, C.E., S. Hormazábal, M. Correa-Ramírez, O. Pizarro, N. Silva, C. Fernández, V. Anabalón & M.L. Torreblanca. 2012. Mesoscale variability and nutrient-phytoplankton distributions off central-southern Chile during the upwelling season: the influence of mesoscale eddies. Prog. Oceanogr., 104: 17-29, doi:10.1016/j.pocean.2012.04.015.

Nauw, J.J., H.M. van Aken, J.R.E. Lutjeharms & W.P.M. de Ruijter. 2006. Intrathermocline eddies in the southern Indian Ocean, J. Geophys. Res., 111, C03006, doi:10.1029/2005JC002917.

Pequeño, G. & S. Sáez. 2000. Los peces litorales del Archipiélago Juan Fernández (Chile): endemismo y relaciones ictiogeográficas. Invest. Mar., Valparaíso, 28: 27-37.

Pingree, R.D. & B. Le Cann. 1992. Three anticyclonic Slope Water Oceanic Eddies (SWODDIES) in the southern bay of Biscay. Deep-Sea Res., 39: 1147-1175.

Pizarro, G., V. Montecino, R. Astoreca, G. Alarcón, G. Yuras & L. Guzmán. 2006. Variabilidad espacial de

condiciones bio-ópticas de la columna de agua entre las costas de Chile insular y continental, primavera 1999 y 2000. Cienc. Tecnol. Mar, 29(1): 45-58.

Richardson, P.L., A.S. Bower & W. Zenk. 2000. A census of Meddies tracked by floats. Prog. Oceanogr., 45: 209-250.

Rozbaczylo, N. & J.C. Castilla. 1987. Invertebrados marinos del Archipiélago Juan Fernández. In: J.C. Castilla (ed.). Islas oceánicas chilenas: conocimiento científico y necesidades de investigación. Ediciones Unversidad Católica de Chile, Santiago, pp. 193-215.

Sasaki, H., M. Nonaka, Y. Masumoto, Y. Sasai, H. Uehara & H. Sakuma. 2008. An eddy-resolving hindcast simulation of the quasi-global ocean from 1950 to 2003 on the earth simulator. In: K. Hamilton & W. Ohfuchi (eds.). High resolution numerical modelling of the atmosphere and ocean. Springer, New York, pp. 157-185.

Sasaki, H., Y. Sasai, S. Kawahara, M. Furuichi, F. Araki, A. Ishida, Y. Yamanaka, Y. Masumoto & H. Sakuma. 2004. A series of eddy-resolving ocean simulations in the world ocean: OFES (OGCM for the Earth Simulator) Project, OCEAN'04, 3, pp. 1535-1541.

Received: 10 March 2014; Accepted: 23 September 2014

Shapiro, G.I. & S.L. Meschanov. 1991. Distribution and spreading of Red Sea Water and salt lens formation in the northwest Indian Ocean. Deep-Sea Res. I, 38: 21-34.

Shchepetkin, A.F. & J.C. McWilliams. 2005. The regional ocean modeling system: a split-explicit, free-surface, topography following coordinates ocean model. Ocean Model., 9: 347-404.

Siegel, D.A., P. Peterson, D.J. McGillicuddy, S. Maritorena & N.B. Nelson. 2011. Bio-optical footprints created by mesoscale eddies in the Sargasso Sea. Geophys. Res. Lett., 38, L133608, doi:10.1029/ 2011GL047660.

Silva, N., N. Rojas & A. Fedele. 2009. Water masses in the Humboldt current system: properties, distribution, and the nitrate deficit as a chemical water mass tracer for equatorial subsurface water off Chile. Deep-Sea Res. II, 56(16): 1004-1020.

Stockner, J.G. 1988. Phototrophic picoplankton: an overview from marine and freshwater ecosystems. Limnol. Oceanogr., 33: 765-775.